^{181}Ta(p,x)^{172}Lu Cross Section Measurements at CNL Using the Stacked Target Method

Sarah Hawkins

January 20, 2023

Abstract

A stack of ^{181}Ta and ^{nat}Cu foils were irradiated using a roughly 67MeV proton beam at Crocker Nuclear Laboratory to obtain nuclear cross section measurements for medically relevant and concurrently produced isotopes. This paper details improvements made to the methodology and experimental setup at CNL for such measurements. Moreover it presents preliminary results for the cross section of ^{181}Ta(p,x)^{172}Lu in the range of 30-65MeV using the variance minimization process for the ^{nat}Cu monitor foils to determine the proton flux through the stack.

1 Introduction

Knowledge of nuclear cross sections fuels the production of medically relevant radioisotopes that are commonly used in the diagnosis and treatment of illnesses like cancer. It dictates the reaction chains and energy ranges that are most efficient for producing these isotopes at a scale feasible for use in the medical field, while simultaneously providing information about isotopes that are concurrently produced. Many concurrently produced isotopes have no benefit to a patient, and some are actively harmful, so they are important to consider. Despite the importance of nuclear cross sections, surprisingly few elements have well-characterized cross sections and thus continued research of both new production reactions and new energy ranges is needed. The stacked target method, as used in this experiment, is one such way to probe novel cross sections.

A cross section is an effective target area, hence the units of cm^2. In nuclear physics, it is energy-dependent and related to the probability that a particular nuclear reaction will take place. This experiment aims to calculate cross sections for natural tantalum, ^{181}Ta irradiated with a proton beam of about 30-65 MeV using the 76" cyclotron housed at Crocker Nuclear Laboratory (CNL). Nuclear reaction notation in the form of A(b,c)D will be used throughout this paper to represent the reaction A + b producing c + D. b and c are commonly light particles, such as a proton represented by "p", meanwhile an "x" indicates unspecified particles. This paper details the preliminary cross section calculations for ^{181}Ta(p,x)^{172}Lu.

The stacked target method was utilized for this experiment, which entails irradiating a stack of thin metal foils with an ion beam to produce different isotopes via nuclear reactions. These isotopes then decay through gamma emission into increasingly stable isotopes.

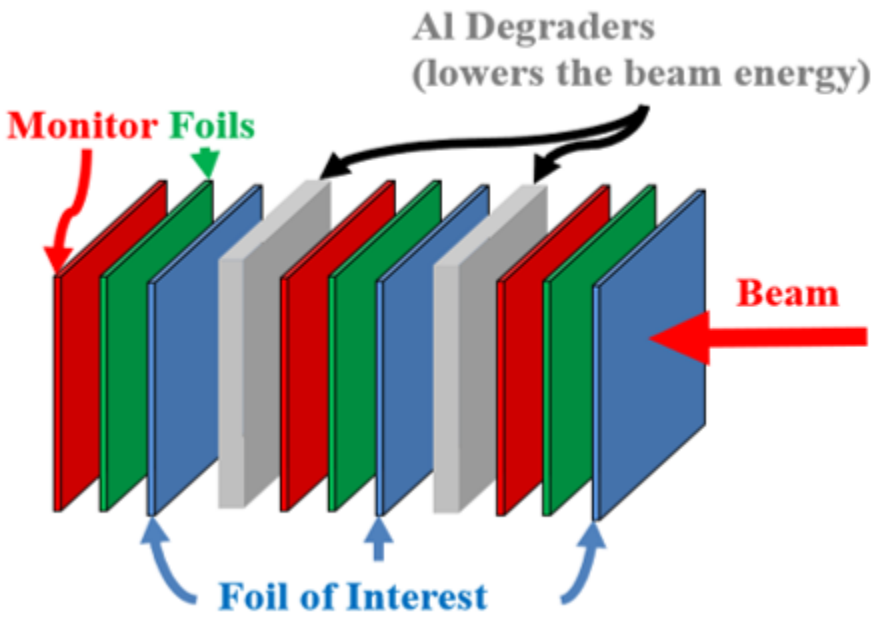

Figure 1: The design of a generic stack utilized for stacked target irradiation. The red and green monitor foils possess a well-known cross section and are used to characterize the beam through the stack. The blue foils of interest, or target foils, have an unknown cross section that is being calculated. The grey Aluminum degarders provide additional degradation of beam energy through the stack [1].

Counting the emitted gamma rays using a high purity Germanium (HPGe) detector allows for calculation of different values relating to the irradiation, including cross sections for each of the produced isotopes.

The benefit of using a stack of foils in a repeating pattern is that the beam energy degrades as it traverses the stack. Thus, a single irradiation allows for a probe of a wider energy range. The design of a generic stack is shown in Figure 1 [1]. As shown, a stack is comprised of monitor foils (green and red), target foils (blue), and additional beam degraders (grey). Monitor foils are selected to have a well-characterized cross section for the given energy range as they are used to calculate the proton flux through the stack. Target foils, in turn, have an unknown or poorly characterized cross section that will be calculated. While every material present in the stack will degrade the beam, additional beam degraders made of aluminum or another material are often included to probe a wider range of energies. The type and thickness of a material dictates how much the beam energy is degraded, as described by the stopping power of an incident particle. Proton transport calculations use these values to calculate the beam degradation at each element in the stack, which is an important measurement as cross section is a function of energy.

This experiment was done in collaboration with the University of California (UC), Berkeley as part of an NSSC summer school being held at UC Davis. They designed a stack consisting of ^{nat}Cu monitor foils and ^{181}Ta target foils, as well as aluminum degraders to further degrade the beam energy.

These Ta target foils are of medical interest due to the production of ^{177}Ta and ^{177}Lu

Figure 2: Left: A model of CNL's 76" cyclotron. Right: A partial image of the cyclotron taken inside the main vault at CNL.

through proton irradiation. These isotopes are being considered as potential cancer treatment due to their ability to emit Auger electrons, which are low-energy electrons emitted by radionuclides during electron capture or other processes [2]. When there is an electron transition to fill a vacancy in an inner orbital, sometimes the resulting energy will be transferred to an outer shell electron instead of being released as a photon. This ejects the Auger electron from the atom with a characteristic energy in the range of several keV. The small size of these Auger electrons relative to nuclei is beneficial as it enables them to target on the level of individual cells [3]. However, more research is needed to study the feasibility of this process in cancer treatment. Thus, it is first necessary to study the production of these Auger-emitting isotopes through cross section measurements, as well as concurrently produced isotopes.

This paper details the parts of this experiment that were undertaken in the summer of 2022 as part of an NSF-funded Research Experience for Undergraduates (REU) at UC Davis. The goal of this research was to improve the experimental setup and methodology used for cross section measurements at CNL. Previously, two stacks - ^{93}Nb target foils in a deuteron beam and ^{59}Co target foils in a proton beam, were irradiated at CNL under air as part of another student's senior thesis, but due to poor statistics and other issues, the analysis was never taken to completion. The successful implementation of a vacuum box at CNL allowed this Ta stack to be the first stack irradiated under vacuum. Due to the timescale of this experiment and the ongoing counting process, a second goal for this research was to obtain a preliminary cross section measurement for the reaction ^{181}Ta(p,x)^{172}Lu, which is concurrently produced alongside the medically relevant isotopes ^{177}Ta and ^{177}Lu.

2 Methodology

2.1 CNL's 76" Isochronous Cyclotron

Irradiation was performed using a proton beam from the 76" isochronous cyclotron housed at CNL, as shown in Figure 2. The basic principle of operation for a cyclotron is as follows.

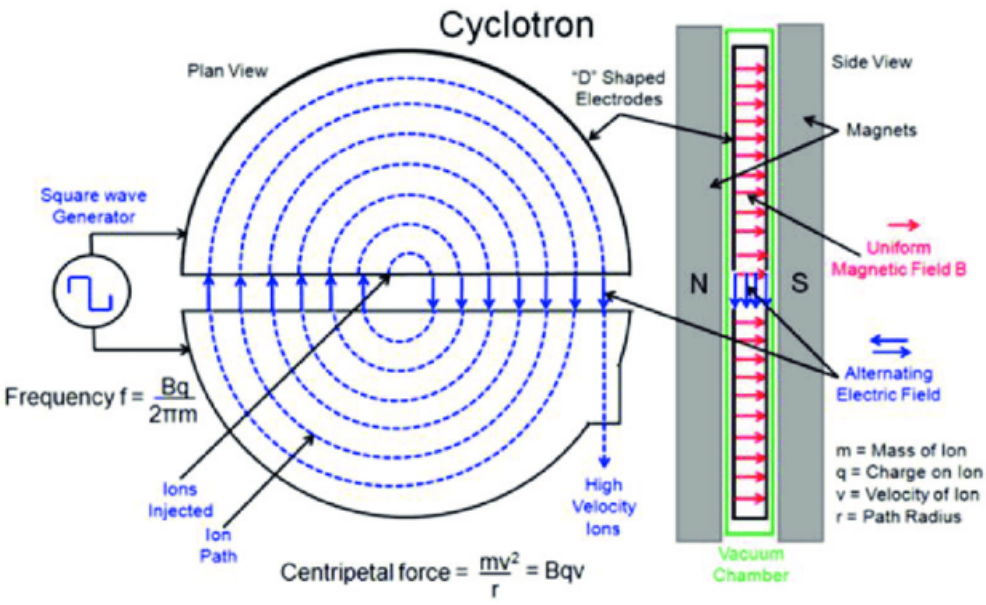

Figure 3: A diagram depicting the basic principle of how a cyclotron operates [4].

An alternating electric field, oscillating at a radio frequency, is applied to the gap between two D-shaped electrodes. Ions are injected into the center and magnets are used to bend the particle's trajectory. Each time the ions cross the the gap, they receives a boost in energy so its radius gradually grows. See Figure 3 [4]. The frequency of these orbits, called the cyclotron frequency f, is given in Equation 1.

$$f = \frac{qB_0}{2\pi m} \tag{1}$$

Here, q is the charge of the ion, B_0 is the magnetic field at the center, and m is the mass of the ion. At relativistic speeds, however, the cyclotron frequency will decrease due to an increase in the particles' relativistic mass. To correct for this, an isochronous cyclotron will vary the magnetic field with radius such that the frequency remains constant. This allows the particles to cross the gap at the same point in the electric field cycle each time.

CNL's cyclotron is capable of a 67.5MeV proton beam, which was utilized for this irradiation, in addition to beams of deuterons, alpha particles, and ^{3}He nuclei. Figure 4 shows the layout of CNL's facility [5]. The orange circle denotes Beam Line 0 inside the main cave, which is where irradiation occurred for this experiment.

2.2 Vacuum Box

A vacuum box was successfully installed in the summer of 2022 in Beam Line 0, which marks a major improvement in the cross section measurement capabilities at CNL and allowed for the Ta stack to be the first stack irradiated at CNL under vacuum. Performing a stacked target irradiation in air introduces additional uncertainty through scattering of the incident protons off air molecules, additional beam degradation through the small "slices" of air between foils, and other processes. Thus, irradiation under vacuum allows for more precise

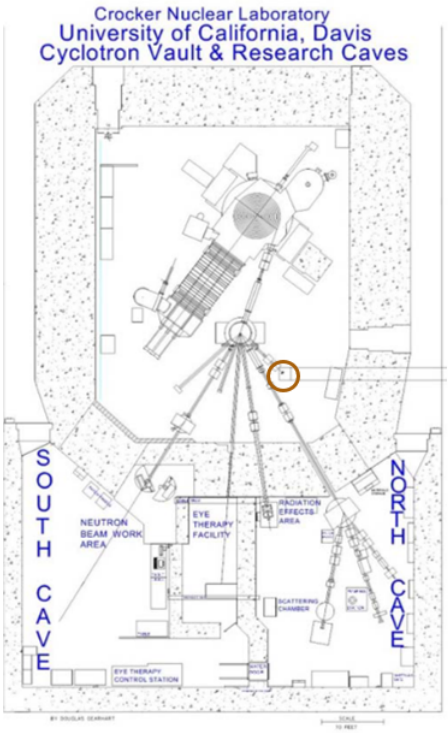

Figure 4: The beam line layout of the CNL cyclotron. The irradiation of the Ta stack was performed in Beam Line 0 (orange circle) [5].

cross section measurements. Figure 5 depicts this box, both with and without its side in place.

Within the vacuum box was an externally controlled motion stage that allowed the Ta stack to be rotated into and out of the beam line during tuning. The wiring of this motion stage to a stepper motor and a limit switch, as well as the programming and calibration for its rotation, was included in this scope of this research.

Due to its location in the main cave, which is inaccessible during irradiation, the stage had to be wired to an external room. This was a multi-step process that required connections to exit the vacuum box, and then exit the main cave to the "chem lab". From there, the connections were soldered to a Raspberry Pi that enabled communication between the stepper motor and the limit switch. Figure 6 depicts the control setup for the motion stage.

The limit switch was located at the 0 position, such that when the stage was directly in the beam line, the switch would close the circuit and send a voltage pulse to the Raspberry Pi indicating its position. From there, the system was calibrated to advance a certain number of "steps" forwards or backwards to rotate the foil stack into or out of position in the beam line. The motion stage also contained a holder for a phosphor screen, which emits photons when exposed to radiation, so calibration included the ability to rotate this phosphor screen into and out of the beam line. A camera was installed beside the vacuum box to both utilize the phosphor screen for visually tuning the beam and confirm that the Ta stack was in position prior to irradiation. All programming was done in Python.

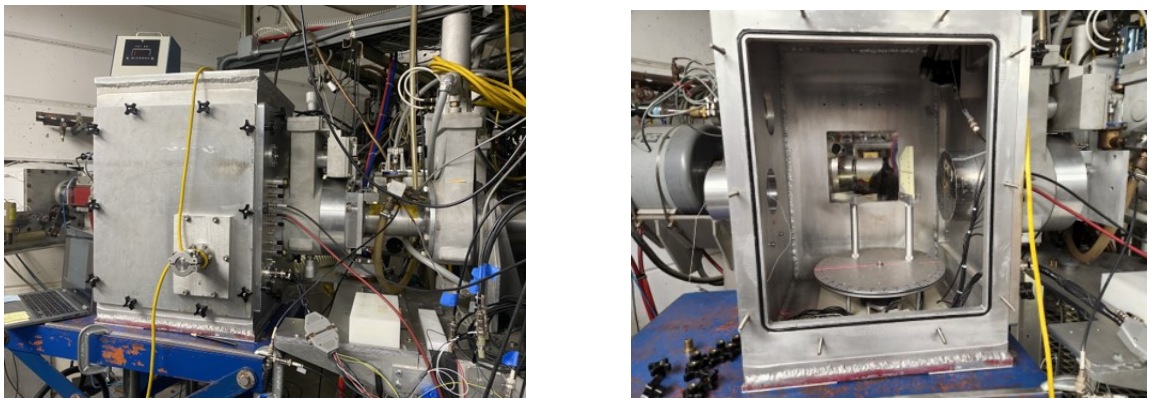

Figure 5: The vacuum box installed in Beam Line 0 with (Left) and without (Right) the final side in place.

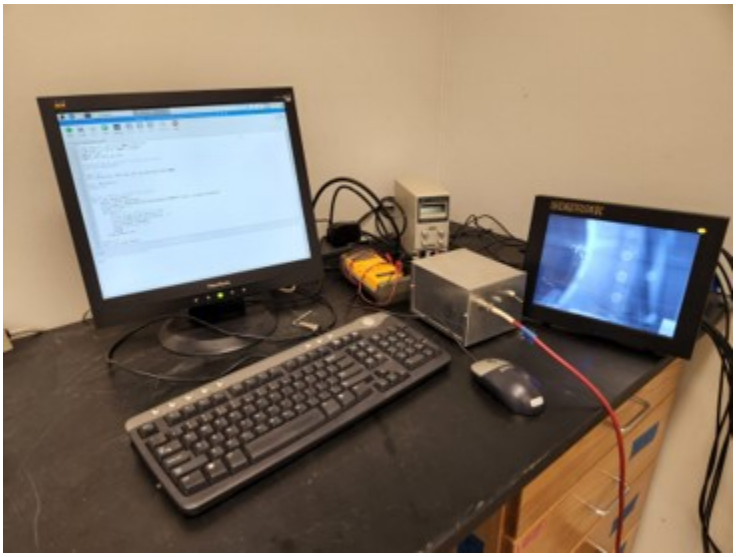

Figure 6: An image of the setup to externally control and view the motion stage while under vacuum.

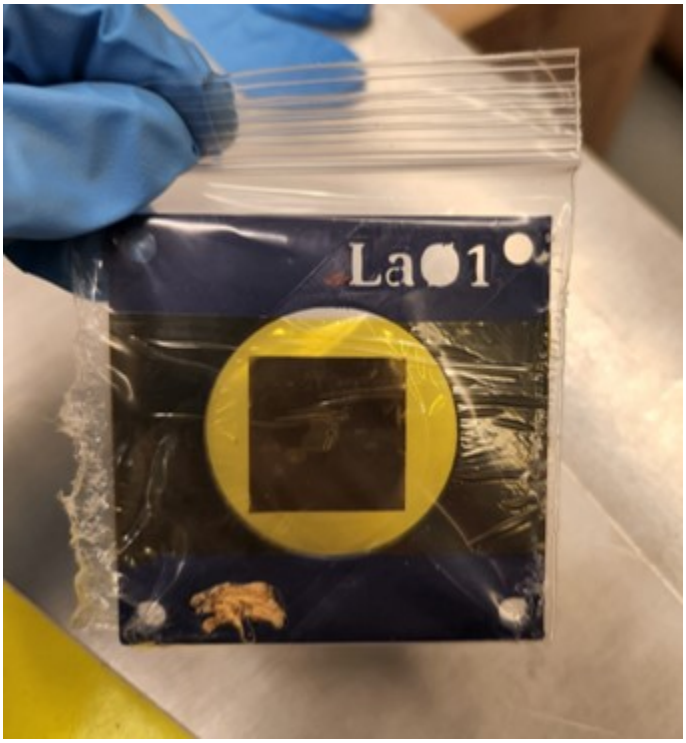

Figure 7: A Ta foil enclosed in kapton tape within a 3D printed holder.

2.3 Stack Design and Irradiation

The stack utilized in this experiment contained 7 ^{181}Ta target foils ($25\mu m$ nominal thickness) and 7 ^{nat}Cu monitor foils ($30\mu m$ nominal thickness). ^{139}La foils were originally planned as the target foil of this experiment, but improper packaging by the vendor left them unusable, so the decision was made to switch to ^{181}Ta. Each of the foils were encapsulated in kapton tape with a silicone adhesive and placed in a 3D printed holder, see Figure 7. The stack also contained 6 aluminum degraders to further degrade the beam energy throughout the stack, as well as two stainless steel foils at the front and back of the stack for delayed Gafchromic film measurements. Additional details about the stack's construction can be found in Appendix A.

Gafchromic film is one method for beam characterization as it changes color when exposed to radiation. It was utilized in this experiment to determine uniformity of the beam spot and its spread as it propagated through the stack. Prior to stack irradiation, a piece of Gafchromic film was directly exposed in Beam Line 0 for about 30 s. A clear and uniform beam spot with sharp edges was produced on the film, as shown in Figure 8 thus indicating good uniformity of the beam. This was later confirmed using ImageJ analysis software.

Stainless steel foils were included on the front and back of the stack for delayed Gafchromic film measurements, which allows for a check on beam uniformity and spread at the time of stack irradiation. Stainless steel absorbs the radiation and holds it in the shape of the beam spot. Following irradiation, a piece of Gafchromic film can be taped to the stainless steel foils and over the course of a couple hours, that radiation will induce a color change on the film in the shape of the beam spot. Thus, a visual of the beam as it enters and exits the stack

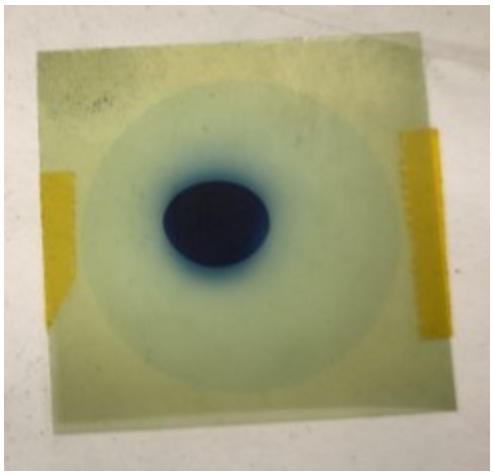

Figure 8: A piece of Gafchromic film directly exposed to a roughly 67MeV proton beam. The sharp edges and consistent color of the beam spot indicate good uniformity.

can be obtained. Figure 9 depicts these two pieces of film. While a much less prominent spot is produced compared to the piece of film directly exposed to the beam, the color appears mostly consistent across the two spots and they are roughly the same shape and size. This again indicates good uniformity of the beam through the stack with very little spread.

This experiment irradiated the stack with a proton beam at 90nA nominal beam current for $t_{irrad} = 4158s$, or about 70 minutes. At the time, a beam energy of about 64MeV was assumed, but recent measurements show that is the beam energy at Beam Line 2. Extrapolating back to Beam Line 0 places the initial energy at 67.3MeV, however work is ongoing to better measure this value. The counting process began roughly 2 hours following the end of irradiation, when people were able to handle the foils safely.

2.4 Gamma Spectroscopy and Counting

The stacked target method utilizes gamma spectroscopy to count the gamma emissions from the produced isotopes. Each foil in the stack is counted independently, and multiple times over a period of weeks or longer to catch both the short-lived and longer-lived isotopes. This experiment used two high purity Germanium (HPGe) detectors - a liquid nitrogen-cooled GMX detector and a mechanically-cooled IDM detector provided by UC Berkeley, to count the 14 Ta and Cu foils. The basic principle of a HPGe detector is as follows.

An unstable isotope can decay via emission of a gamma ray at a characteristic energy. This gamma will interact with the Ge crystal through ionization to produce an electron-hole pair. An electric field is applied to the crystal, which causes the pair to drift to opposing electrodes and creates a voltage pulse. Figure 10 depicts a diagram of this process [6]. The amplitude of the pulse is proportional to the energy of the incident gamma ray, and will be read out using a multi-channel analyzer (MCA). Using a software called Maestro, the number of pulses as each energy will be counted. This allows for identification of isotopes, as different isotopes will emit gamma rays at certain characteristic energies.

Counting of the foils began approximately 2 hours following irradiation using the GMX and IDM detectors. The setups for both are shown in Figure 11. Foils were initially counted

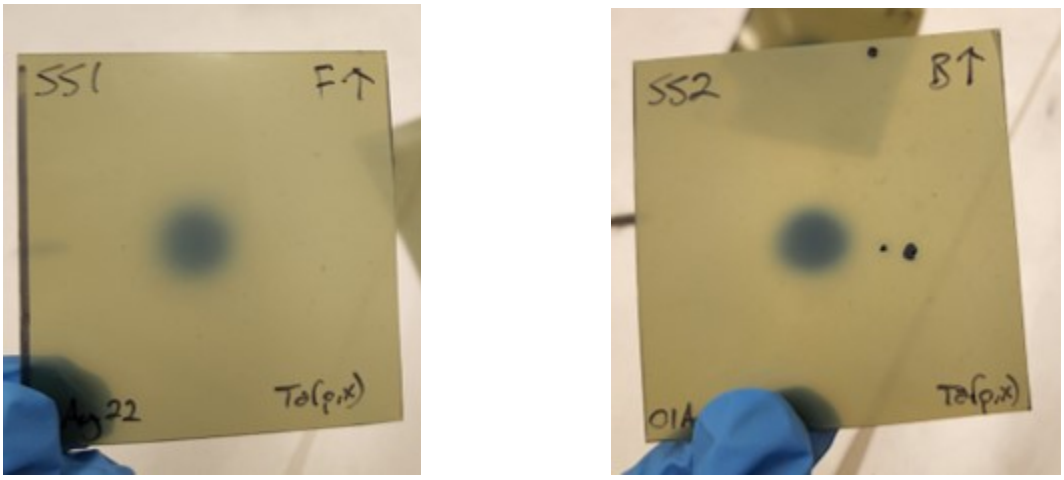

Figure 9: The results of delayed Gafchromic film measurements using stainless steel foils on the front (Left) and back (Right) of the stack. Both are of similar size, shape, and color consistently which indicates good uniformity and little spread of the beam as it propagated through the stack.

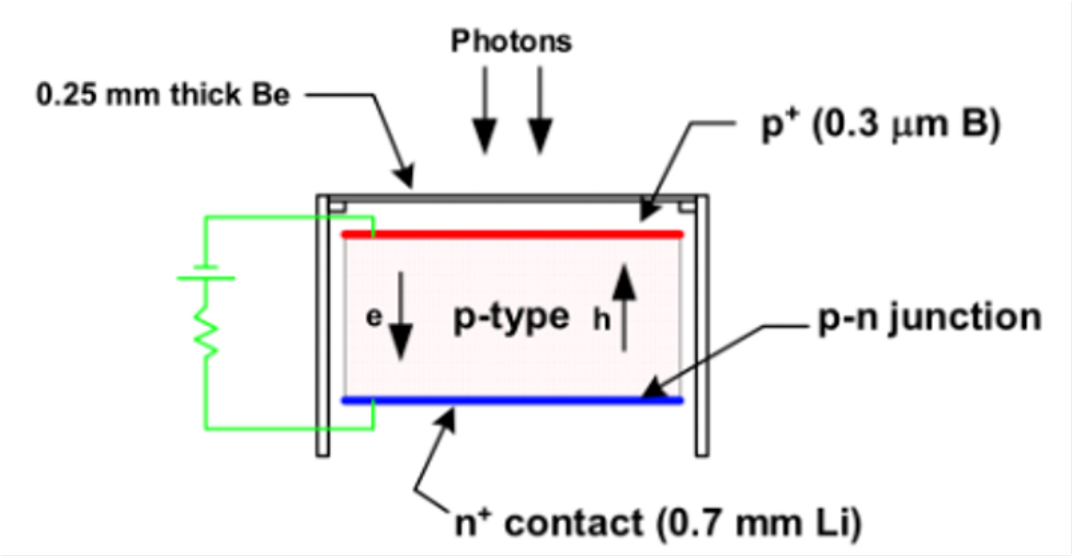

Figure 10: Diagram of how a HPGe detector operates [6].

Figure 11: The two HPGe detectors utilized for counting. Left: The GMX detector housed at CNL. Right: The IDM detector provided by UC Berkeley.

Element	Mass Number
Hf	170, 171, 172, 173, 175, 177m, 179m, 180m
W	174, 175, 176, 177, 178, 179, 181
Ta	172, 173, 174, 175, 176, 177, 178, 180
Lu	170, 171, 172, 176m, 177, 177m, 179
Yb	175

Table 1: List of isotopes that were expected to be observed in the ^{181}Ta spectra.

to about 10 minutes to observe the shorter-lived isotopes before they decayed away. The foils were then rotated back in for progressively longer counts, starting at about 1 hour each and having progressed to 12-24 hours at a time as of the end of the REU. The counting process is still ongoing, so all results presented here will be preliminary.

There were 5 isotopes of interest in the ^{nat}Cu monitor foils, as recommended by the IAEA; ^{62}Zn, ^{63}Zn, ^{65}Zn, ^{56}Co, ^{58}Co [7]. There were 20-30 isotopes of interest that were likely to be observed in the ^{181}Ta target foils, and they are listed in Table 1. Their characteristic gamma rays cover an energy range of about 0-3keV, so ^{181}Ta foils were given preference for time on the IDM detector, since it has much better resolution than the GMX. The ^{nat}Cu foils were counted using both the GMX and the IDM, but due to operational issues with the GMX that brings into question the validity of the data it collected, all GMX data is excluded from this analysis. The goal of this experiment is to obtain cross section measurements for each of the Ta-produced isotopes that are observed. This research in particular, however, focused on ^{172}Lu, which has a half-life of $t_{1/2} = 6.70$days.

3 Data Analysis

The majority of the data analysis was completed using the Python library Curie, which was designed by Jonathan Morrell at UC Berkeley specifically for the analysis of experimental nuclear data [8]. The following sections outline the general process for analyzing both the monitor and target foil data to calculate a cross section for the production of a given isotope [9–12]. There will also be a discussion of the results of this research, which used ^{nat}Cu monitor foils focused on the reaction ^{181}Ta(p,x)^{172}Lu. All results presented here are preliminary, and the complete suite of cross section measurements for the observed isotopes will presented in a forthcoming paper.

3.1 Calibration and Peak Fitting

Calibration of the HPGe detectors was the first step in the data analysis process. Channel number of the MCA was correlated to the energy of the incident gamma ray by using standard, calibration sources with a known activity. Standard calibration sources, commonly ^{152}Eu or ^{137}Cs, emit distinct characteristic gamma rays over a range of energies. By knowing the activity of the source, it is possible to predict the ideal spectra of the source if it was incident on an ideal detector. Through comparison of that ideal spectra and what is actually observed using the detector at hand, the detector can be calibrated appropriately. For this reason, a point source is preferred to reduce uncertainty in the solid angle of the incident gamma rays. This process also allows for calibration of the detector's efficiency, ϵ, which is the ratio of the number of gamma rays detected to the number of gamma rays incident on the detector [6]. While an efficiency calibration is only valid at a single distance from the detector, corrections can be applied to the solid angle for spectra taken at other distances.

Calibration spectra were taken for both the GMX and IDM detectors after the initial foil counting using a ^{152}Eu point source. The counting was repeated at several different distances from the detectors to improve the accuracy of the calibration. A drastic change in the results from the GMX data was observed after including these updated calibration spectra into the analysis, which suggests major issues with the GMX data and led to the decision to exclude it.

Using Curie's calibration function, these spectra were then fit to their source and respective detectors. Figure 12 displays an example calibration spectra from the IDM detector with the source placed at 48cm.

Following calibration, each of the spectra taken for each of the foils must be analyzed. The first step here is to identify the gamma peaks in each spectrum for a given isotope and fit them using a Gaussian function. Curie has a fit_peaks() function to identify and fit peaks for a given isotope, which was heavily utilized in this research for its convenience. It also returned the number of counts in a given peak, which is an important measurement for the rest of the data analysis process.

However, it was important to review Curie's results as there are several instances where Curie's peak fitting fails. This includes poorly fitted peaks due to the smearing of neighboring peaks or a low count rate in the peak, as well as multiple gammas from different isotopes existing at a single energy. Two basic cuts were applied to the data to ensure proper peak fitting; a minimum number of counts, N, in the peak and a maximum on the χ^2 value. I

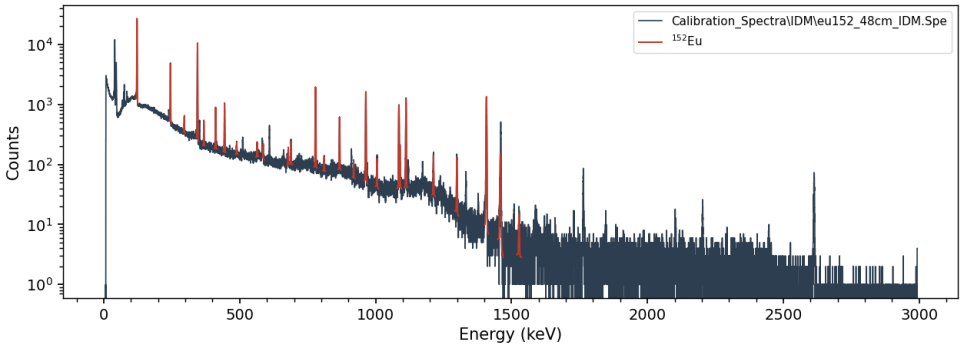

Figure 12: Calibration spectra for the IDM detector with the ^{152}Eu source placed at a distance of 48cm.

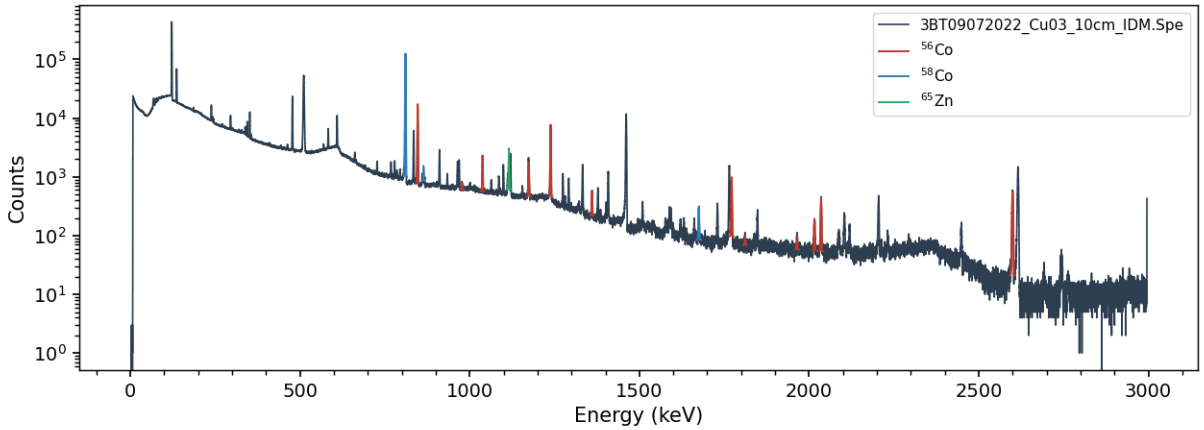

Figure 13: An example ^{nat}Cu spectrum for Cu03 at a distance of 10cm. The observed isotopes ^{56}Co (red), ^{58}Co (blue), and ^{65}Zn (green).

dictated that $N_{Cu} > 100$, $N_{Ta} > 500$, and $\chi^2 < 10$. I also manually removed several peaks at a specific gamma energy due to consistently incorrect fitting.

The ^{nat}Cu monitor foils only had a handful of observed peaks resulting from isotopes of interest, an example of which is in Figure 13. The ^{181}Ta foils, however, had a much larger number of peaks and many that were coincident with one another. An example is shown in Figure 14.

This research specifically focused on the production of ^{172}Lu. Figure 15 depicts an example ^{181}Ta spectrum from Foil 5 with just ^{172}Lu highlighted in red. Care was taken to remove any poorly fitted peaks from the data set. The remaining peaks had characteristic energies at 203.433keV, 264.798 keV, 270.028 keV, 366.684 keV, 372.507 keV, 410.308keV, 432.549 keV, 490.437 keV, 540.187 keV, 551.078 keV, 709.133 keV, 810.064keV, 912.079 keV, 1002.74 keV, 1022.37 keV, 1093.63keV, 1113.05 keV, 1402.53 keV, 1488.94 keV, 1542.85 keV, 1584.12 keV.

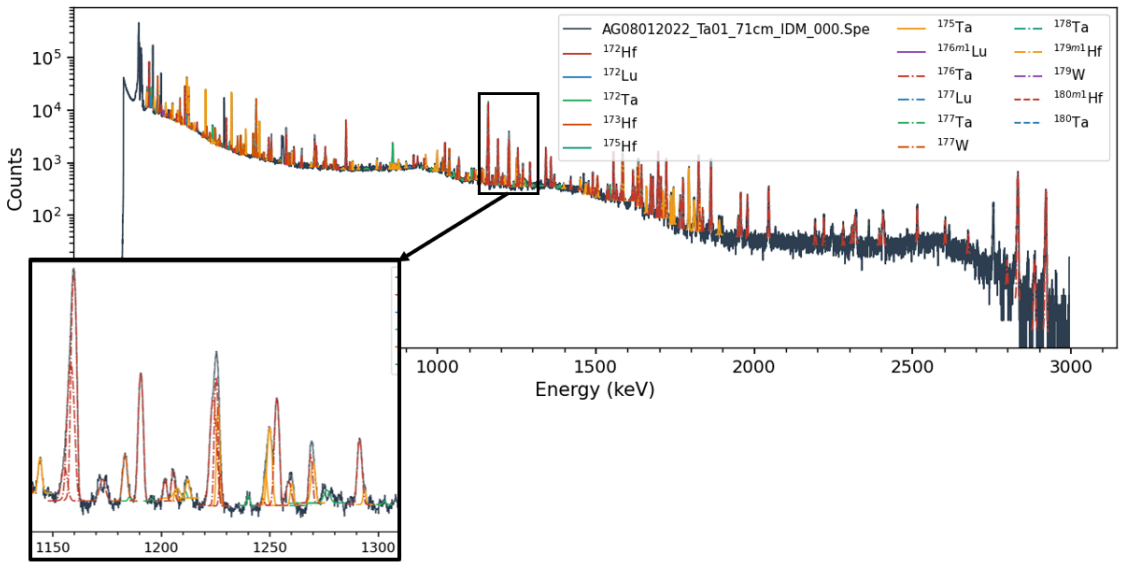

Figure 14: An example ^{181}Ta spectrum for Ta01 at a distance of 71cm. The spectrum includes only a portion of isotopes that are expected to observed throughout the counting process. The image zooms in to the region of 1150 - 1300 keV to display examples of both well-fitted peaks and neighboring peaks that are so close that they cannot be resolved and so must be removed.

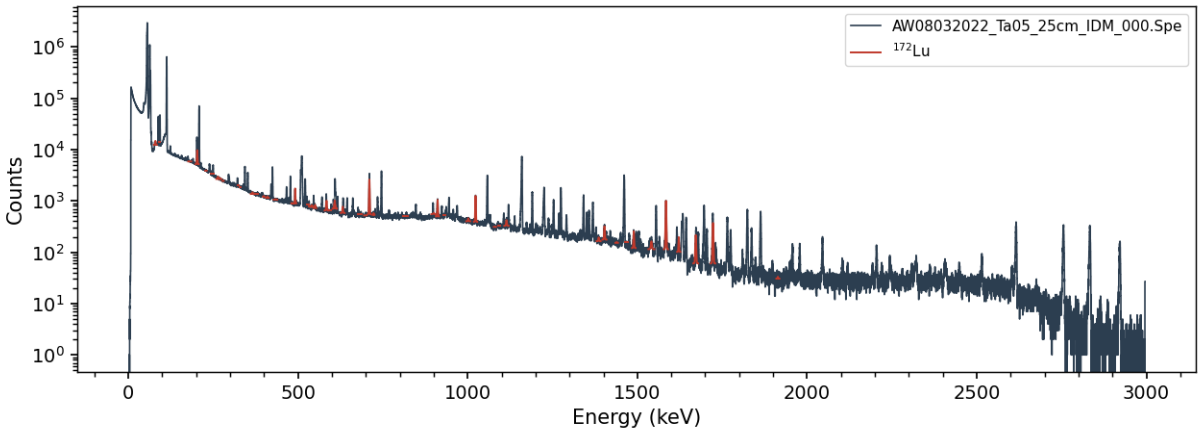

Figure 15: An example ^{181}Ta spectrum of Ta05 at 25cm with just the peaks of ^{172}Lu highlighted red.

3.2 Production Rate Calculations

Curie's peak fitting function returns information about each of the peaks that were fit, including the number of counts, or the number of gamma rays detected at that energy. This information enables calculation of the end-of-bombardment (EOB) activity of the foil, A_0, and it's production rate, R.

The activity of a radioactive material is the rate of its decay into more stable isotopes, and is commonly given in units of Becquerels, Bq, or Curie, Ci. Over time, the activity is governed by the fundamental law of radioactive decay, such that the activity, A at some time t can be written:

$$A(t) = A_0 e^{-\lambda t} \tag{2}$$

Here, λ is the decay constant of the material $[s^{-1}]$ and the EOB activity can be expressed as:

$$A_0 = R(1 - e^{\lambda t_{irrad}}) \tag{3}$$

t_{irrad} is the duration of irradiation, which is $t_{irrad} = 4158s$ in this experiment. The production rate, R, refers to the rate at which an isotope is produced during the irradiation. It is an important quantity that is dependent on the particle flux of the incident beam, I_p [protons per second], the areal number density of the foils, ρr $[cm^{-2}]$, and the cross section σ $[cm^2]$.

$$R = I_p(\rho r)\sigma \tag{4}$$

Curie's fit_R() function will return the production rate for a specified isotope by fitting these relations to the count data obtained through peak fitting. It will also take the decay chain of the specified isotope, specifically any daughter products, into consideration and include that in its calculation. This process was repeated for each isotope of interest in each of the foils, as the production rate is a necessary quantity for the remainder of the data analysis process.

Curie is also capable of returning activity plots for each of its calculations, which can provide a quick visual check that the data is being correctly fitted. From this, it was observed that there may be some issues with the production rate calculation for ^{172}Lu, as the activity curve does not seem to accurately fit all of the points in a couple foils. Additional analysis will need to be done in this step to determine why the fit seems to exclude some data points.

The uncertainty in the production rate calculation is calculated by Curie in the form of the covariance matrix to the fit. For the purposes of this research, the uncertainties generated by Curie or calculated through standard error propagation were sufficient.

3.3 Proton Flux and Variance Minimization

The next step is to calculate the proton flux through the stack using the ^{nat}Cu monitor foils. The monitor foils were chosen to have well-characterized cross sections, such that the production rate formula can be rearranged to solve for proton flux, I_p.

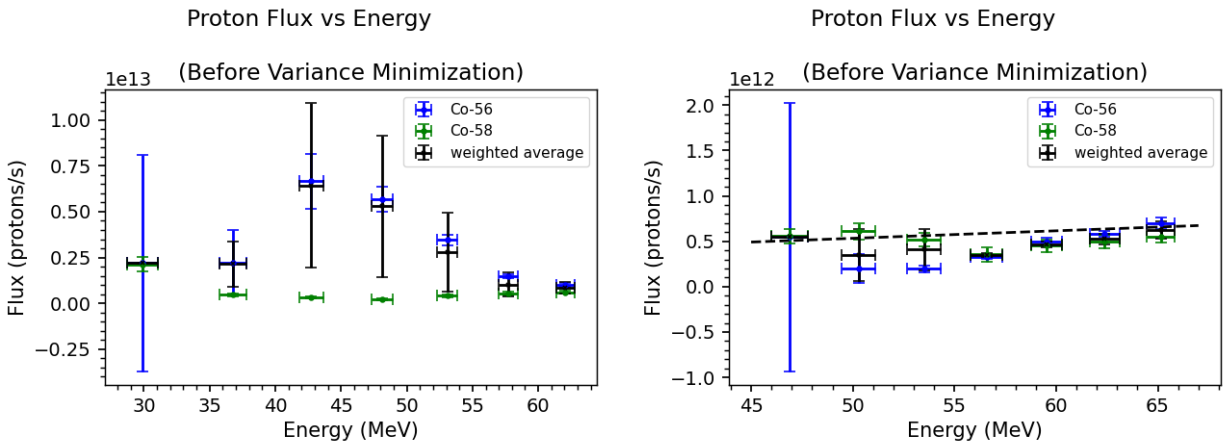

Figure 16: The proton flux calculated as a function of energy through the stack for ^{56}Co (blue) and ^{58}Co (green) before (left) and after (right) the variance minimization process. A weighted average (black) was also included

$$I_p = \frac{R}{(\rho r)\sigma} \tag{5}$$

For this reason, only the monitor foils are considered when calculating proton flux. This method results in a more accurate calculation compared to simply inputting the nominal proton flux of the beam, since both the beam energy and the number of protons incident on each foil degrades through the stack. Following calculation of the flux at each foil, the data can be linearly fit to determine the flux at each element of the stack. The result is an energy-dependent proton flux value at each of the target foils, thus giving better cross section calculations.

The uncertainty in proton flux was obtained by adding the following uncertainties in quadrature, as dictated by standard error propagation techniques: uncertainty in the Curie-calculated production rate, ΔR, uncertainty in the areal number density of the foil, $\Delta(\rho r)$, uncertainty in the IAEA recommended cross section, $\Delta\sigma$, uncertainty in the decay constant, $\Delta\lambda$, and uncertainty in the irradiation time which was conservatively estimated at $\Delta t_{irrad} = 60s$. The last two values are generally negligible, but were included for completion.

The IAEA recommends 5 monitor reactions for ^{nat}Cu foils in a proton beam; ^{62}Zn, ^{63}Zn, ^{65}Zn, ^{56}Co, and ^{58}Co. Initial counts of the monitor foils were performed by the GMX detector, and several weeks following the end of irradiation, counting was continued the IDM. Of the 5 monitor reactions, only 2 were observed in the IDM spectra; ^{56}Co and ^{58}Co. Thus, only these reactions were considered in this analysis.

The left hand image in Figure 16 depicts the initial calculated proton flux for each of the observed monitor isotopes through the stack. A weighted average for each foil was also included (black). These results, however, are nonphysical. The proton flux should gradually decrease towards the back of the stack, i.e. at lower energies. This is not observed as all the isotopes are shown to increase beyond their initial value at lower energies. ^{56}Co displays this most prominently with its spike in Foil 5.

The issue stems from the proton transport calculations that are used to determine the

energy of each element in the stack. These predict a distribution of different energies that are incident on each stack element. However, as the beam degrades towards lower energies, the width of this distribution spreads due to so called "energy straggling". Thus there is a greater uncertainty in the beam energy at each foil towards the back of the stack.

Variance minimization, which has been detailed more thoroughly in papers by Jonathan Morrell and Andrew Voyles [10–12], is a technique that accounts for the poorly characterized transport calculations and reduces uncertainty in the energy assignment of each foil. It relies on the assumption that the proton flux calculations for different monitor reactions in each foil should be constant. By treating the effective density of a stack element, such as the aluminum degraders or kapton tape, as a free parameter, its value can be varied such that it minimizes the variance of the monitor reactions present in a foil. It is important to note that this technique is simply a corrective measure to improve the energy determination at each foil in the stack, and does not indicate erroneous measurements of the density of the stack element being varied.

The last foil in the stack is the most sensitive to perturbations in the proton transport calculations since it is located at the lowest energy. As such, the variance of the observed monitor reactions is typically minimized with respect to this last foil.

This analysis approached the variance minimization process in a somewhat untraditional manner and performed the process twice; once varying the initial beam energy and once for the density of the aluminum degraders. Performing variance minimization for the initial beam energy was a stopgap solution to the need for a more precise measurement of the initial beam energy. It will not be performed in the final analysis of this data as research is being done to obtain such a measurement.

In this analysis, the initial beam energy was varied between $60 - 75$MeV, with its nominal value being 64MeV. This was the assumed energy in Beam Line 0 at the time of the experiment, and was thus used in parts of this analysis. Figure 17 plots the variance against the energy of the foil over which it is being minimized for both Foil 5 (left) and Foil 7 (right). Over this variation, the minimum of the variance for Foil 7 was located at $E_7 = 30$MeV, which corresponds to the nominal $E_0 = 64$MeV. However, it seemed to be approaching a second minimum at higher energies. Moreover, such a result does not resolve the issue of the peak of ^{56}Co in Foil 5. Thus, the variance was minimized with respect to Foil 5, which corresponded to an initial energy $E_0 = 70.5$MeV. While this is a higher energy than the cyclotron is capable of reaching, recent measurements do suggest that the beam energy should be higher than 64MeV. Thus, the decision was made to set $E_0 = 67$MeV, which corresponds to just below the maximum achievable proton energy.

Using this value, the variance minimization process was repeated, this time varying the thickness of the aluminum degrader between $0.8 - 2.0$mm. Figure 18 shows that with respect to Foil 7, the variance has a local minimum that corresponds to the nominal degrader thickness of $a = 1.6$mm. The variance reaches the global minimum at $E_7 = 47$MeV and this corresponds to a aluminum degrader thickness $a = 0.95$mm.

Thus, using initial energy $E_0 = 67$MeV and aluminum degrader thickness $a = 0.95$mm, I re-calculated the proton flux through the stack. The right hand image in Figure 16 shows the results, which are much improved compared to initial calculations. The flux generally decreases through the stack, and as such a linear fit could be applied to describe the general behavior of the flux through the stack. However, there are still issues with this process that

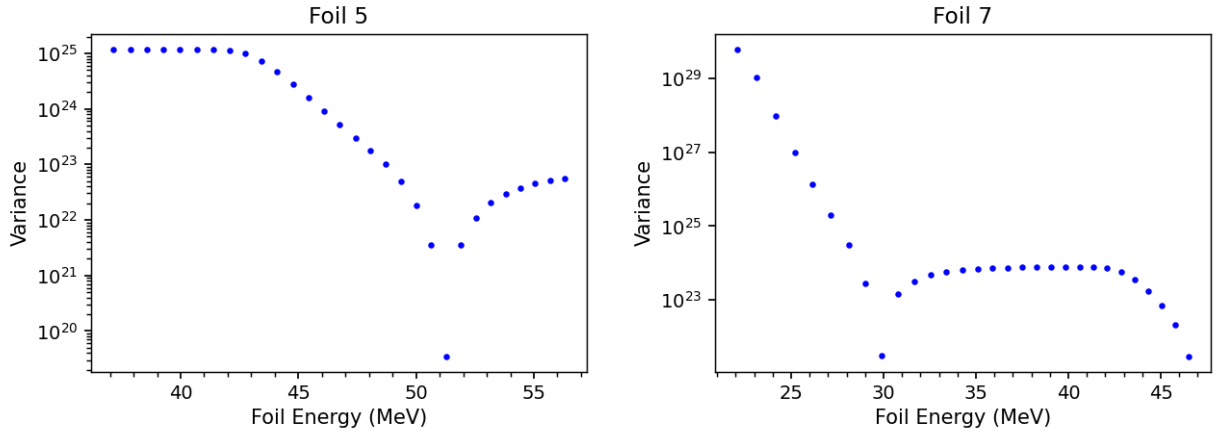

Figure 17: Results of the initial energy variance minimization. The variance of the proton flux, which thus has units of $(protons/s)^2$ is plotted against foil energy for Foil 5 (left) and Foil (7). Foil 5 reaches a minimum at $E_5 \approx 51$MeV, which corresponds to $E_0 = 70.5$MeV. Foil 7 has a local minimum at $E_7 = 30$MeV, corresponding to $E_0 = 64$MeV.

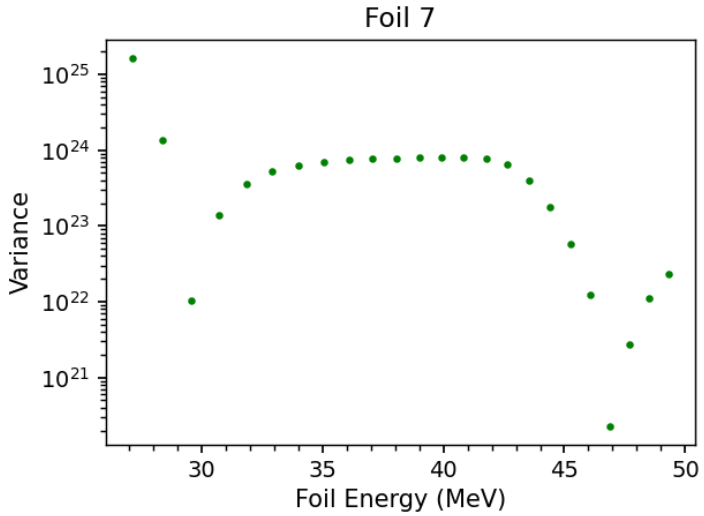

Figure 18: Results of aluminum degrader thickness variance minimization. The variance, with units of $(protons/s)^2$ was minimized with respect to Foil 7.

will need to be better understood prior to completion of the final analysis. In particular, while the flux at Foil 7 is still less than at Foil 1, there still seems to be a bit of a minimum in the middle of the stack instead of a consistent decrease. Around that minimum in Foils 5 and 6, the agreement between the ^{56}Co and ^{58}Co isn't as strong as other Foils. There are also the large error bars for the ^{56}Co measurement for Foil 7, all of which suggests the need for a more stringent variance minimization process.

However, these results will suffice for this preliminary measurement. At such, the equation of the linear fit, given in Equation 6 was used to describe the propagation of the flux, I_p, as a function of energy, E through the stack. The energy should be given in units of MeV to obtain a proton flux in units of protons per second. The uncertainty in the parameters of the fit equation are quite large, but these should be better understood and reduced through additional analysis.

$$I_p = E(3.9 \pm 2.1) \times 10^9 + (1.3 \pm 1.2) \times 10^{11} \tag{6}$$

3.4 ^{181}Ta(p,x)^{172}Lu Cross Section Calculation

The final step is to calculate the cross section for the isotope of interest in each of the target foils, again using a rearranged version of Equation 4.

$$\sigma = \frac{R}{I_p(\rho r)} \tag{7}$$

The proton flux, I_p is obtained through variance minimization of the proton flux calculations from monitor reactions in the monitor foils. Thus, the cross section calculation is only for the target foils.

It is important to make a distinction between cumulative and independent cross sections. An independent cross section makes a distinction between the isotopes that are produced directly from irradiation of the foils, and that which are produced through decay chains. Such a distinction is not always possible depending on the decay schemes of the isotopes of interest and their half lives. A cumulative cross section does not make that distinction, and is the type being calculated in this research.

As such, the cross section calculated in this paper for ^{181}Ta(p,x)^{172}Lu will include the production of ^{172}Lu as a result of irradiation and that from the decay of ^{172}Hf. In turn, ^{172}Hf can be produced during irradiation or from the decay ^{172}Ta. Decay schemes quickly become very complex when considering so many isotopes, hence the decision to calculate a cumulative cross section. However, it is possible to conclude that the majority of the ^{172}Lu observed thus far was produced via irradiation. ^{172}Lu has a half life of $t_{1/2} = 6.70$days, while ^{172}Hf, the parent isotope in its decay chain, has a half life of $t_{1/2} = 1.87$years. Thus, very little of the produced ^{172}Hf would have decayed in the first couple weeks of counting.

Figure 19 presents the preliminary cross section plot for the production of ^{172}Lu. Again, the results presented here are all preliminary given that data analysis and counting is still ongoing. While the error bars are significant, these will hopefully be reduced through continued collection and analysis of data. In particular, improving the variance minimization process and having a better understanding of the proton flux through the stack would improve the results.

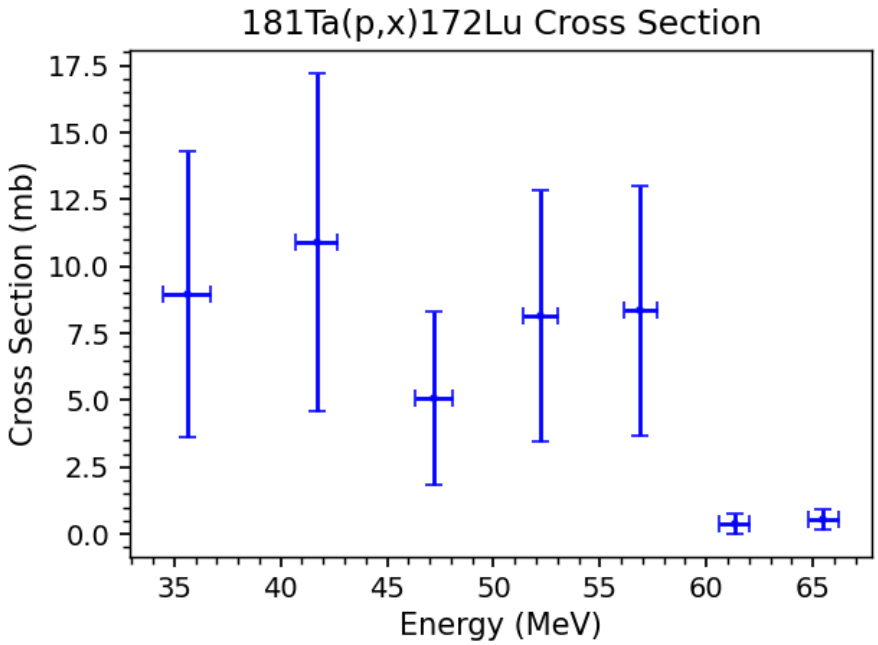

Figure 19: Preliminary plot of the cross section as a function of energy for ^{181}Ta(p,x)^{172}Lu.

However, these results are still significant because this experiment marks the first measurement of the cross section for ^{181}Ta(p,x)^{172}Lu in the energy range of $35-65$MeV. Previous measurements were made by Medvedev, D.G. et al in 2008 [13] and Michel, R. et al in 2002 [14], but they utilized much higher initial energies. They observed cross sections between 5 and 10 mb in the range of about 100 to 2,000MeV, which is of similar magnitude to the cross sections measured in this research. However, Michel's data in particular is plagued by very large uncertainties. Model predictions for this reaction predict that the cross section should be 0 in the energy range of $35-65$MeV, but these preliminary results suggest that this is not the case, which could have implications for the production of medically relevant isotopes from ^{181}Ta in this region.

4 Conclusion

This research improved the experimental setup at CNL through the successful implementation of a motion stage within the vacuum box that can be connected to Beam Line 0. This will allow for more nuclear cross section measurements to be performed at CNL in the future, including repeating prior measurements made with Nb and Co stacks for improved results.

It also calculated preliminary results for the cross section of ^{181}Ta(p,x)^{172}Lu in the energy range of $35-65$MeV. Using the stacked target method, a stack of ^{181}Ta target foils and ^{nat}Cu monitor foils were irradiated using a roughly 67MeV proton beam. Over the course of the following weeks, the gamma decays of the isotopes produced in the foils were counted using HPGe detectors. However, in this analysis all data from the GMX detector was excluded due

to issues with its operation that brought into question the validity of the data it collected.

The python library Curie was heavily utilized in the analysis of the data, which included fitting the characteristic gamma energies of the isotopes and calculating their production rate. Using the IAEA recommended monitor reactions ^{nat}Cu(p,x)^{56,58}Co, the proton flux through the stack was calculated. This required performing a variance minimization process to correct for uncertainties in the proton transport calculations. This analysis repeated this process for both the initial beam energy and the aluminum degrader thickness and found that the variance was minimized at $E_0 = 67$MeV and $a = 0.95$mm. Such a process produces more physical results for the proton flux, and allowed for a linear fit to be applied. This fit allows for a better understanding of the proton flux incident on each foil in the stack. As such, this result was plugged into the calculation of the cross section for ^{181}Ta(p,x)^{172}Lu.

A preliminary measurement of the cross section of ^{181}Ta(p,x)^{172}Lu was reported, which marks the first measurement in this energy range. The production of ^{172}Lu would be a background process in the production of medically relevant isotopes from ^{181}Ta, such as ^{177}Ta and ^{177}Lu. Models predict no cross section for this reaction in this energy range, but this analysis measures a clear, albeit small cross section for the production of ^{172}Lu. This is significant and could have implications for using ^{181}Ta for the production of medically relevant isotopes.

However, improvements will need to be made to this analysis process prior to the publication of final results. In particular, work is ongoing to obtain a better measurement of the initial beam energy. Recent beam measurements that allowed for extrapolation back to Beam Line 0 placed the beam energy around 67.3MeV, so it should certainly be higher than the 64MeV that was initially assumed. This should improve the results of the variance minimization, as the process will only have to be completed once for the aluminum degrader thickness, but a better understanding of the process as a whole will be necessary for determining the proton flux through the stack. Understanding this is vital for cross section results, and is currently the largest source of uncertainty. Thus, there remains work to be done in this analysis.

5 Acknowledgements

I'd like to thank Eric Prebys, Lena Korkeila, Michael Backfish and the rest of the CNL control room for welcoming me to CNL and for their continual guidance and support this summer. None of this would have been possible without their help. I'd also like to thank Jonathan Morrell and Andrew Voyles for their collaboration and expertise in this experiment.

A Additional ^{181}Ta Stack Information

Table 2 contains the full details of the stack utilized in this experiment, including RMS thickness and areal density of the foils. The kapton and silicone stack elements compose the adhesive kapton tape that secured the foils to their holders, and the aluminum was utilized as a beam degrader. Only the nominal thickness was provided for these elements, hence

their poor characterization and inclusion in the variance minimization process.

Table 2: The full details of the ^{181}Ta stack that was irradiated in this experiment. Measurements were taken by Andrew Voyles and Jonathan Morell at UC Berkeley.

Target Layer	**RMS Thickness** (μm)	**Areal Density** (mg/cm^2)
Stainless Steel - SS1	250 ± 1.0	194.555 ± 0.565
Kapton	25	
Silicone	63	
Tantalum - Ta01	19.5 ± 1.3	27.136 ± 0.270
Silicone	63	
Kapton	25	
Kapton	25	
Silicone	63	
Copper - Cu01	30.5 ± 0.6	22.287 ± 0.093
Silicone	63	
Kapton	25	
Aluminum - D1	1600	
Kapton	25	
Silicone	63	
Tantalum - Ta02	24.5 ± 1.0	27.348 ± 0.262
Silicone	63	
Kapton	25	
Kapton	25	
Silicone	63	
Copper - Cu02	24.9 ± 5.2	22.191 ± 0.138
Silicone	63	
Kapton	25	
Aluminum - D2	1600	
Kapton	25	
Silicone	63	
Tantalum - Ta03	21.5 ± 1.3	27.517 ± 0.292
Silicone	63	
Kapton	25	
Kapton	25	
Silicone	63	
Copper - Cu03	30.0 ± 0.0	22.273 ± 0.055
Silicone	63	
Kapton	25	
Aluminum - D3	1600	
Kapton	25	
Silicone	63	

Continued on next page

Table 2 – continued from previous page

Target Layer	RMS Thickness (μm)	Third column
Tantalum - Ta04	22.3 ± 1.7	27.148 ± 0.272
Silicone	63	
Kapton	25	
Kapton	25	
Silicone	63	
Copper - Cu04	29.8 ± 0.5	22.277 ± 0.101
Silicone	63	
Kapton	25	
Aluminum - D4	1600	
Kapton	25	
Silicone	63	
Tantalum - Ta05	20.4 ± 2.4	27.289 ± 0.175
Silicone	63	
Kapton	25	
Kapton	25	
Silicone	63	
Copper - Cu05	30.3 ± 0.5	22.177 ± 0.172
Silicone	63	
Kapton	25	
Aluminum - D5	1600	
Kapton	25	
Silicone	63	
Tantalum - Ta06	23.1 ± 2.6	27.223 ± 0.138
Silicone	63	
Kapton	25	
Kapton	25	
Silicone	63	
Copper - Cu06	30.0 ± 0.0	22.245 ± 0.093
Silicone	63	
Kapton	25	
Aluminum - D6	1600	
Kapton	25	
Silicone	63	
Tantalum - Ta07	21.3 ± 1.0	26.970 ± 0.146
Silicone	63	
Kapton	25	
Kapton	25	
Silicone	63	
Copper - Cu07	29.8 ± 1.3	22.150 ± 0.080
Silicone	63	
Kapton	25	
Stainless Steel - SS2	124.5 ± 1.0	101.336 ± 0.229

References

[1] Bernstein, L.A, "Nuclear Data from Berkeley to Baghdad - Playing with the BAND" in *San Diego State University Colloquium.* (2021).

[2] Uusijärvi, H. et al. Electron- and Positron-Emitting Radiolanthanides for Therapy: Aspects of Dosimetry and Production. *Journal of Nuclear Medicine*, 47, 5, 807-814 (2006).

[3] Ku, A., Facca, V.J., Cai, Z. et al. Auger electrons for cancer therapy – a review. *EJNMMI radiopharm. chem.* 4, 27 (2019). https://doi.org/10.1186/s41181-019-0075-2

[4] Ortun, A. Introductory Chapter: Accelerators and Colliders (June 2020), https://doi.org/10.5772/intechopen.93068

[5] Hartman, S.C. UC Davis 76 Inch Isochronous Cyclotron: Radiation Effects Infrastructure, *UC Davis* (March 2016).

[6] Knoll, G.F. Radiation Detection and Measurement, *John Wiley Sons* (2000).

[7] A. Hermanne et al., Nucl. Data Sheets 148 (2018) 338-382

[8] Morrell, J.T., Curie, (2022) jtmorrell.github.io/curie/.

[9] Springer, A. Investigation of production cross sections, using stacked targets at the 88" Cyclotron with focus on ^{nat}Fe(p, x)^{51}Mn. *Master of Science in Physics University of California Berkeley* (2017). arXiv:1707.05908v1 [nucl-ex].

[10] Voyles, A.S. et al. Excitation functions for (p,x) reactions of niobium in the energy range of Ep=40–90MeV, *Nuclear Instruments and Methods in Physics Research Section B: Beam Interactions with Materials and Atoms*, 429 53-74 (2018). https://doi.org/10.1016/j.nimb.2018.05.028.

[11] Morrell, J.T., Voyles, A.S., Basunia, M.S. et al. Measurement of 139La(p,x) cross sections from 35–60 MeV by stacked-target activation. *Eur. Phys. J. A* 56, 13 (2020). https://doi.org/10.1140/epja/s10050-019-00010-0

[12] Chapman, R.K. et al. Measurement of the 160Gd(p,n)160Tb excitation function from 4–18 MeV using stacked-target activation, *Applied Radiation and Isotopes* 171 (2021). https://doi.org/10.1016/j.apradiso.2021.109647.

[13] Medvedev, D.G, et al. Activation of natural Hf and Ta in relation to the production of 177Lu, *Applied Radiation and Isotopes* 66 (2008). http://dx.doi.org/10.1016/j.apradiso.2008.02.090

[14] Michel, R. et al. Cross sections for the production of radionuclides by proton-induced reactions on W, Ta, Pb and Bi from thresholds up to 2.6 GeV. *Journal of Nuclear Science and Technology* 39 (2002) http://dx.doi.org/10.1080/00223131.2002.10875084